Characterization of nonlinear ultrasonic diffuse energy imaging

Jack Potter and Anthony Croxford

***Abstract*—Nonlinear ultrasonic diffuse energy imaging is a highly sensitive method for the measurement of elastic nonlinearity. While the underlying principles that govern the technique are understood, the precise behavior and sensitivity have not previously been quantified. This article presents experimental, theoretical and numerical modeling studies undertaken to characterize nonlinear diffuse energy imaging. The influence of incoherent noise, elastic nonlinearity and instrumentation error are quantified. This work enables prediction of spatial sensitivity, aperture and amplitude dependence of the measurement, all of which moves the technique towards industrial viability. Further, while previous studies have focused on detection of closed cracks, the ultimate aim for nonlinear ultrasonic imaging in application to material testing is the detection of damage precursors, which requires a sensitivity to weak classical nonlinearity. This study identifies the experimental requirements necessary for this to be achieved, greatly expanding the potential applicability of nonlinear ultrasonic array imaging.**

I. Introduction

The measurement of elastic nonlinearity is of importance to a number of fields. In application to the nondestructive testing of materials, the microstructural changes that form in advance of macroscopic damage exhibit a weak, classical nonlinear elastic response[1]. Furthermore, other discrete defects such as closed cracks and kissing bonds exhibit a strong non-classical nonlinear response as a consequence of contact-acoustic effects[2]. Detection of damage at earlier stages both increases safety and allows for cost reduction by increasing the necessary length of inspection intervals. Great interest also exists within the field of bio-medical imaging for which nonlinearity has been found to be strongly correlated with pathological changes in tissue.

Regardless of the underlying mechanics, the effect of nonlinear elasticity on a propagating ultrasonic field is some form of spectral distortion. The fundamental challenges of nonlinear ultrasonic measurements come from the weakness of this effect and from the difficulty of isolating the source of spectral distortion spatially. Many techniques have been developed for nonlinear ultrasonic inspection. Classical techniques typically excite the field and measure distortions using monolithic transducers. The most prevalent of these methods are harmonic generation[3] and wave mixing[4], [5]. Harmonic generation considers the self-interaction of a longitudinal wave and provides a measurement proportional to the integral of elastic nonlinearity along the propagation path of the wave. Wave mixing techniques involve the interaction of two or more incident waves. If the mode, frequencies and wave vectors are selected to satisfy certain specific phase matching criteria then a secondary scattered wave is generated at either the sum or difference frequencies of the incident waves. Since the secondary wave is only generated at the intersection of the incident waves, a degree of nonlinear localisation is achieved. The effective imaging resolution is however limited by the size of the interaction volume. Further, the complicated experimental requirements of such methods limit their practical applicability.

A focus of much work in recent years has been on the development of techniques that use ultrasonic phased arrays for imaging elastic nonlinearity. This has been motivated primarily due to the ability of ultrasonic arrays to easily generate specifically designed interference patterns within a material and to remotely isolate the source of scattered waves. The primary application of these techniques has been the imaging of discrete defects such as tightly closed cracks. Such defects exhibit a very strong localized nonlinear response and consequently the imaging of which presents a much less challenging problem than the weak nonlinearity associated with damage precursors. The most common approach adopted to this problem has been the detection of distortion within the portion of the field scattered coherently from the inspection point. Most commonly sub- or superharmonic components of the signal are analyzed[6], [7], [8]. Other techniques seek to modulate a parameter of the system and examine changes within the transmission bandwidth of the back scattered signal. These modulation parameters have included static load[9], temperature[10] and amplitude of the transmitted signal[11]. These coherent scattering techniques recover only a small proportion of the total information pertaining to elastic nonlinearity that is encoded onto the field. This is because they can only analyze the part of the field that happens to be scattered back to the receiver from the inspection point. Information contained within the rest of the field is lost.

An array imaging technique has previously been proposed that measures nonlinearity without a reliance on a backscattered signal and is known as nonlinear ultrasonic diffuse energy imaging[12]. This technique infers the elastic nonlinearity at a point in space by contrasting the diffuse energy of the ultrasonic fields produced by sequential and parallel focusing at that point. This method has been shown to be highly sensitive to fatigue cracks, being capable of accurate detection and sizing at very early stages of crack growth[13]. Within the class of array imaging techniques, nonlinear diffuse energy imaging is uniquely positioned for application to damage precursor detection since there is no backscatter

The authors are with the Department of Mechanical Engineering, University of Bristol, Queen's Building, University Walk, Bristol, BS8 1TR, United Kingdom. Email: jack.potter@bristol.ac.uk

associated with classical forms of nonlinearity. Further, there is no fundamental physical reason to negate its application to these problems, limitations are instead due to practical experimental considerations. As with any conventional imaging technique, in order to demonstrate industrial viability a process of characterization must be undertaken. A crucial part of this is the determination of sensitivity to elastic nonlinearity, from which the experimental requirements for damage precursor measurement may be obtained. The purpose of this study is to obtain an understanding of the behavior and sensitivity of nonlinear diffuse energy imaging.

II. Nonlinear diffuse energy imaging

The theory of nonlinear diffuse energy imaging, as described by [12], will first be reviewed. An ultrasonic phased array may be operated in two main modes of transmission. Firstly there is classical physical beamforming, for which elements are triggered in parallel with the application of some relative phase delays. In this case some designed interference pattern (often a steered or focused beam) is physically formed within a specimen. The second mode of transmission is what is commonly referred to as full matrix capture [14]. In this case elements transmit sequentially and the responses for each transmitter-receiver pair are collated to form the so-called full matrix. The interference effects of the classically beamformed parallel transmission can be emulated by applying phase delays in post-processing of the full matrix, resulting in synthetic beamforming. The parallel and sequential transmission modes are illustrated in Fig. 1. The sequential capture approach to array imaging relies on an assumption of linear superposition and for linear systems, in the absence of random noise, the two methods are exactly equivalent. In the presence of elastic nonlinearity the propagation of these parallel and sequential fields differ, an effect which may be exploited in making nonlinear measurements.

When a parallel field is focused, the material physically sees higher stress at the focal spot than in any of the individual transmission cycles of a sequential capture. Since, by definition, a nonlinear system loses proportionality, there is a higher flux of energy from the transmission bandwidth due to nonlinearity at the focal point for a parallel field. Since generally the inspection point is inaccessible to the measurement system this relative nonlinear loss cannot be measured directly and must be inferred through some other measurement of the field.

Parallel and sequential fields have identical linear propagation, identical transmission energy and, where there is no interference between element transmissions, identical nonlinear self-interaction effects. The only differences in propagation occur as a consequence of interference between the fields produced by different element transmissions, which is an effect dominated by the focal point. Consequently, after the focal time, the difference in total system energy in the transmission bandwidth between parallel and sequentially focused fields is approximately equal to that which occurred through nonlinear losses at the focal point. If the total energy (within the transmission bandwidth) of the system could be measured for the parallel and sequential focusing cases, then the difference between the two values would provide a measure of elastic nonlinearity at the focal point.

Measurement of total system energy for the early-time, coherent field is not feasible since it would require the field to be measured at every point. The total energy may however be inferred through analysis of the subsequent diffuse field. Sometime after initial transmission of sound, the field will homogenize as a consequence of multiple scattering. In this state energy is statistically uniform throughout the system and the statistical diffuse energy measured at any point is proportional to the total energy in the system. Furthermore, the relative loss of energy that occurred at the focal point is spread uniformly. Consequently, the relative diffuse energy of parallel and sequentially focused fields is proportional to the relative energy loss at the focal point which in turn is a function of the elastic nonlinearity at that location. This is the operating principle of the nonlinear diffuse energy imaging technique, the metric for which is defined as the normalized difference in sequential and parallel diffuse energy. This metric, for inspection location $\bar{r}_f$, may be written as follows[12]

$$\gamma(\bar{r}_f) = \frac{E_s(\bar{r}_f) - E_p(\bar{r}_f)}{E_s(\bar{r}_f)}, \tag{1}$$

where E_p and E_s are the parallel and sequential diffuse energy values respectively. Experimentally the sequential energy term is obtained through integration of diffuse energy across the transmission bandwidth, averaged across all receiving elements. For an array of N elements and center frequency ω_0 this may be expressed as

$$E_s(\bar{r}_f) = \sum_{j=1}^{N} \left(\int_{\frac{2}{3}\omega_0}^{\frac{4}{3}\omega_0} \left| \sum_{k=1}^{N} F_{k,j}(\omega) e^{-i\omega\delta_k(\bar{r}_f)} \right|^2 \mathrm{d}\omega \right), \tag{2}$$

where $F_{k,j}(\omega)$ is the complex valued frequency spectra of the diffuse full matrix for which the indices k and j denote transmission and reception elements respectively. $\delta_k(\bar{r}_f)$ is the delay applied to element k required to achieve focusing at point $\bar{r}_f$. The $2/3\ \omega_0$ evaluated bandwidth is the largest for which there is no internal movement of energy. Similarly, the diffuse parallel energy, E_p, is given by

$$E_p(\bar{r}_f) = \sum_{j=1}^{N} \left(\int_{\frac{2}{3}\omega_0}^{\frac{4}{3}\omega_0} \left| H_j(\bar{r}_f, \omega) \right|^2 \mathrm{d}\omega \right), \tag{3}$$

where $H_j(\bar{r}_f, \omega)$ is the diffuse spectra of the signal received on the j element when all elements are transmitted in parallel with delays $\delta_k(\bar{r}_f)$.

In order to demonstrate the properties of the technique an experimental imaging example is considered. A closed fatigue crack was grown within an aluminium test piece. A 5 mm diameter hole was machined behind the crack tip alongside a second hole to provide a reference. This test block was designed to approximate fatigue crack growth initiated at a fixing hole. Full details of its preparation are available[12]. Inspection was conducted using an Imasonic (Voray-sur-l'Ognon, France) 64 element ultrasonic array with

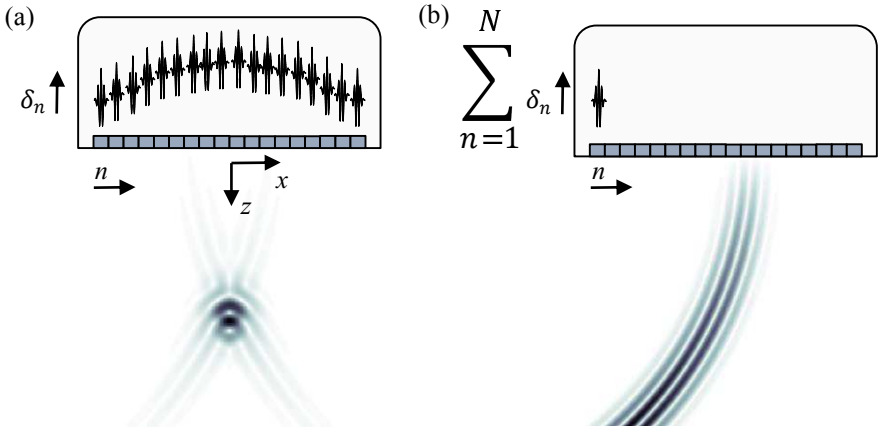

Fig. 1. Schematic illustration of (a) parallel and (b) sequential field focusing.

a nominal centre frequency ω_0 of 5 MHz and pitch of 0.63 mm, in conjunction with a Micropulse FMC model array controller manufactured by Peak NDT Ltd (Derby, UK). To obtain a diffuse field a reception delay of 0.1 ms was applied and energy was evaluated over a window length of 0.12 ms.

Selection of reception delay represents a compromise between field diffusivity and signal to noise ratio. If the reception delay is too small then the statistical conditions that the measurement requires (most importantly the spatial homogeneity of the field) are not satisfied, resulting in imaging artefacts. Conversely, if the delay is too long then random noise dominates the received signal and the effective dynamic range of the acoustic measurement is reduced. Longer window lengths allow the statistical properties of a diffuse state to be reached at earlier times but increase the computational expense of the measurement. In this case, the window length used is the maximum that the instrument can acquire in a single capture.

Typical nonlinear and linear images acquired for this sample are shown in Fig. 2. The linear image can be seen to be dominated by the back wall and hole reflections. Some evidence of the defect is provided by shadowing effects on the left hole caused by diffraction at the crack tip. This shadowing effect can be seen a slight null on the left hole reflection in comparison with the undamaged hole. This is however an unclear indication and no sizing information is present. The nonlinear image shows only a clear indication from the defect as a consequence of the local nonlinear elastic response. Note the complete absence of back wall and hole reflections within the nonlinear image. This excellent linear suppression is a direct consequence of the diffuse energy measurement. Since imaging is not based upon a coherently scattered signal from the inspection point, instrument and material nonlinearity do not produce artifacts from linear features as is the case with coherent nonlinear imaging techniques. This is important since a geometric feature which acts as a stress raiser to initiate crack growth is itself inherently a strong linear scatterer. Consequently, without separation of linear and nonlinear modalities, a small defect can be masked by the feature it grows from.

The high sensitivity of the nonlinear metric is derived from two aspects of the measurement. Firstly, by measuring the energy flux from the transmission bandwidth, the movement of energy to any frequency component is captured making the metric broadly sensitive to any underlying nonlinear mechanics. Secondly, the nature of the diffuse measurement is such that regardless of spatial directivity of energy flux (be it purely a distortion of the forward propagating field or some nonlinear scattering phenomena), it contributes to the measured value. This implicitly provides a full reception aperture around every inspection point.

The measurement is predicated on the hypothesis that information pertaining to elastic nonlinearity at the focal point is preserved in the relative diffuse energy of parallel and sequential fields. In order to move the technique towards industrial viability it is necessary to precisely quantify the degree to which elastic nonlinearity and other factors contribute towards the experimentally acquired metric in addition to determining the ultimate measurement capability. Broadly, the factors contributing to the measured γ value may be grouped into three terms as follows

$$\gamma(\bar{r}_f, \bar{r}) = \eta(\bar{r}_f, \bar{r}) + p + e(\bar{r}), \tag{4}$$

where $\eta(\bar{r}_f, \bar{r})$ represents the contribution of elastic nonlinearity. This includes the effect from both the focal point and the wider material contributions. This determines the localisation of the measurement in addition to spatial sensitivity. p is the contribution of incoherent noise to the measurement and finally $e(\bar{r})$ contains the remaining experimental error, most significantly effects of instrumentation nonlinearity and repeatability, and is the term which ultimately determines the limit of experimental sensitivity. The focus of this work is the characterization of these terms.

III. Incoherent noise

Firstly, the effect p of incoherent noise on the measurement shall be considered. Incoherent noise is a zero-mean random process. For conventional linear or nonlinear imaging based on the recorded amplitude of a scattered wave, incoherent noise appears directly as noise within the image space. In this case, because the evaluated quantity is statistical energy the

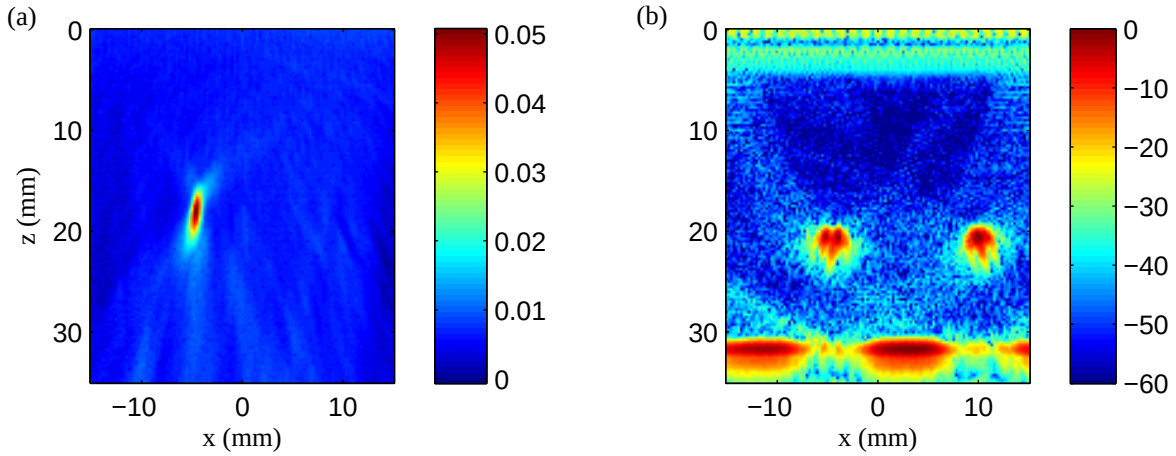

Fig. 2. Experimental images (a) nonlinear metric γ (b) linear (total focusing method) (dB)

effect of random noise is different. Random noise has a non-zero mean contribution on the measured energy value which is, in a statistical sense, spatially independent. Further, the relative contribution of noise is not equivalent for parallel and sequential focusing. Consequently the effect of noise is not removed in the subtraction process, leading to an offset in the resulting nonlinear image.

Let A be a parameter proportional to the acoustic energy of a single sequential response and let the energy due to random noise be some quantity ϵA, such that total expected energy of a sequential measurement is $E\left[F_{k,j}^2\right] = A(1+\epsilon)$. For a given level of random noise the value of ϵ will decrease as the amplitude of A increases. For a diffuse field this energy is independent of transmitting and receiving elements. For a parallel measurement the acoustic energy of each response is N times that of a sequential measurement however the noise energy is the same such that $E\left[H_j^2\right] = A(N+\epsilon)$.

If an idealised diffuse field is assumed then both inter-element responses and noise are uncorrelated. In this case all statistical energy terms will add independently when the individual fields are summed. In reality the diffuse responses of the full matrix are weakly correlated but this is a small effect. Under these assumptions, the evaluated parallel energy summed across all receiving elements would be

$$E_p = AN(N+\epsilon). \tag{5}$$

Similarly, once the post-processed focusing is applied by delaying and summing across transmitters, the sequential energy is

$$E_s = AN^2(1+\epsilon). \tag{6}$$

Relating these terms to the imaging metric γ, the contribution of noise to the image is found to be

$$p = \frac{E_s - E_p}{E_s} = \frac{(N-1)\epsilon}{N(1+\epsilon)}, \tag{7}$$

which has the limit

$$\lim_{N\to\infty} p(N) = \frac{\epsilon}{1+\epsilon}. \tag{8}$$

Consequently, for $\epsilon \ll 1$, the image offset due to incoherent noise is expected to approach a value of approximately ϵ as the number of transmitting elements increases. The energy in the received signals acquired when no sound is transmitted by the array is due to random noise. The ϵ value may therefore be found experimentally by evaluating the energy received by the array in sequential transmission operation, which contains the acoustic and noise energy values, relative to the energy received when operated passively (that is the energy of the signal recorded when no sound is transmitted), which contains only noise. This measured energy value can be contrasted to the value measured using a sequential transmission to find the experimental ϵ value. For the previously described experimental example this is found to be $\epsilon = 0.009$. Eq. (7) is plotted in Fig. 3(a) for this example. It is clear that for the large number of elements of a typical ultrasonic array (in this case 64), the image offset due to incoherent noise will be close to ϵ.

The influence of element number on the baseline measurement, γ_0, is evaluated experimentally through a series of tests increasing the transmission aperture symmetrically about the centre. The baseline value is taken as the rms γ within an undamaged region of material. This relationship is shown in Fig. 3(b) and demonstrates the type of asymptotic response predicted by the analysis of incoherent noise.

If the sequential measurements are acquired using a number of experimental averages equal to the number of elements, N, the noise energy will be reduced by a factor of N relative the acoustic energy such that $E\left[F_{k,j}^2\right] = A(1+\epsilon/N)$. For this case, the sequential energy E_s term then becomes equivalent to parallel energy E_p obtained with no averaging. Applying N averages to the sequential acquisition only should therefore remove the statistical effect of incoherent noise from the resulting nonlinear image. This would also be equivalent to a $\sqrt{N}$ relative increase in reception gain for sequential captures

$$\rho_0 \frac{\partial^2 u_i}{\partial t^2} - \mu \frac{\partial^2 u_i}{\partial x_k \partial x_k} - \left(K + \frac{\mu}{3}\right) \frac{\partial^2 u_l}{\partial x_l \partial x_i} = \left(\mu + \frac{A}{4}\right) \left(\frac{\partial^2 u_l}{\partial x_k \partial x_k} \frac{\partial u_l}{\partial x_i} + \frac{\partial^2 u_l}{\partial x_k \partial x_k} \frac{\partial u_i}{\partial x_l} + 2 \frac{\partial^2 u_i}{\partial x_l \partial x_k} \frac{\partial u_l}{\partial x_k}\right) + \left(K + \frac{\mu}{3} + \frac{A}{4} + B\right) \left(\frac{\partial^2 u_l}{\partial x_i \partial x_k} \frac{\partial u_l}{\partial x_k} + \frac{\partial^2 u_k}{\partial x_l \partial x_k} \frac{\partial u_i}{\partial x_l}\right) + \left(K - \frac{2}{3\mu} + B\right) \left(\frac{\partial^2 u_i}{\partial x_k \partial x_k} \frac{\partial u_i}{\partial x_l}\right) + \left(\frac{A}{4} + B\right) \left(\frac{\partial^2 u_k}{\partial x_l \partial x_k} \frac{\partial u_l}{\partial x_i} + \frac{\partial^2 u_l}{\partial x_i \partial x_k} \frac{\partial u_k}{\partial x_l}\right) + (B + 2C) \left(\frac{\partial^2 u_k}{\partial x_i \partial x_k} \frac{\partial u_l}{\partial x_l}\right), \tag{9}$$

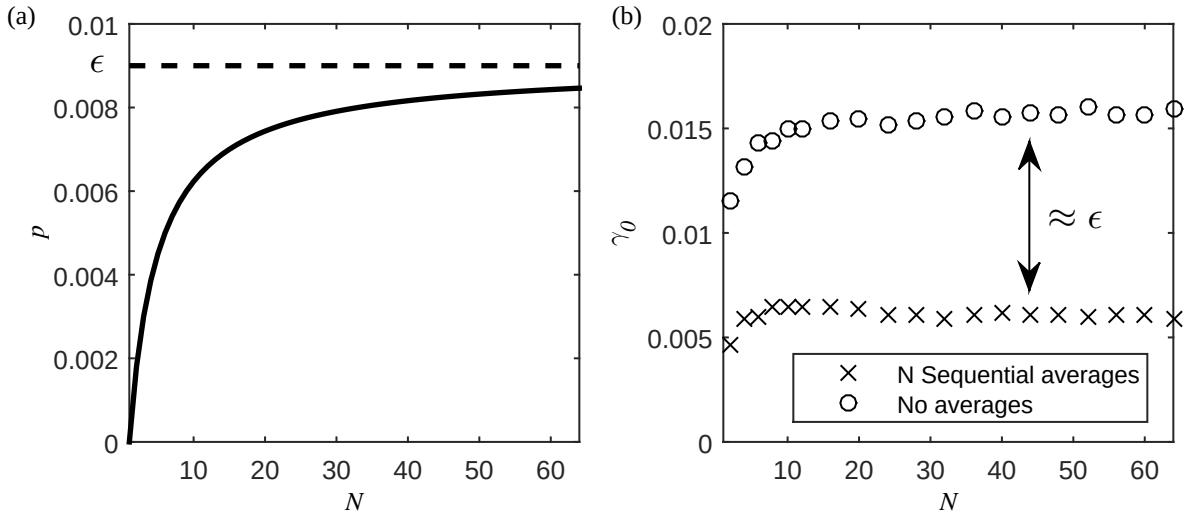

Fig. 3. (a) Theoretical incoherent noise contribution, p (b) Experimental baseline measurement.

but only if all the incoherent noise appears after the gain stage of the signal chain.

The experimental study of the baseline nonlinear measurement was repeated with the inclusion of N sequential averages, the results of which are plotted in Fig 3(b). It is seen that the effect of averaging is to reduce the baseline measurement for large element numbers by very close to the measured ϵ value. This is consistent with the previous analysis and suggests that the effect of random noise on the nonlinear measurement is both well understood and, despite the weak acoustic signals associated with diffuse measurements, can be largely removed. The remaining baseline measurement ($\gamma \approx 0.005$) is expected to comprise of nonlinear material effects and instrumentation error.

It should be noted that noise is still detrimental to the measurement since, as a consequence of bit-rate limits, the acoustic information lost through signal quantization increases proportionally with noise. Additionally, if the noise is not perfectly uncorrelated (as is common with periodic electromagnetic interference), this approach will not completely remove the contribution to the baseline value. All subsequent experimental results are obtained using N sequential averages.

IV. Modeling

The term η which describes the influence of elastic nonlinearity on the measurement is now considered. The imaging metric, γ, captures the total nonlinear energy loss from the transmission bandwidth. The relative parallel-sequential energy loss which occurs as the fields propagate through the focal point is preserved in the relative diffuse energy. The difference in total energy of the parallel and sequential coherent fields is equivalent to that of the diffuse fields. Consequently, in order to find the nonlinear elastic contribution to the metric, it is not necessary to model the diffuse field itself. The relative nonlinear energy loss need only be computed for the early time, coherent component of the field. Modeling is undertaken in order to quantify the relative energy flux produced when an array is focused in a nonlinear elastic medium.

Previous experimental studies have examined nonlinear diffuse energy imaging in application to fatigue cracks[12], [13]. The measured nonlinear response in those examples is almost certainly due predominantly to non-classical contact acoustic effects. The ultimate aim of this form of nonlinear imaging however is in application to damage precursor detection. This requires sensitivity to weak, classical elastic nonlinearity. To this end, the dependence of nonlinear diffuse energy imaging on third order elastic strain energy is considered. The governing partial differential equation for such a system is given by Eq. (9)[4], where ρ_0 is the material density and K and μ are the bulk and shear moduli respectively. A, B and C are the Landau-Lifshitz third order elastic constants[15]. Alternatively these may be expressed in terms of the Murnaghan constants [16] as $l = B + C$, $m = A/2 + B$ and $n = A$.

A. Incident field

A perturbative approach is adopted to the solution of Eq. (9) in which the displacement field $\bar{u}(t, \bar{r})$ is considered as the

$$\bar{U}^{(0)}(\bar{r},\omega) = \Delta(2\pi c_l/\omega_0)^{1/2} T(\omega) \sum_{n=1}^{N} \Bigg\{ \bar{A}_n(\bar{r}) D_{Ln}(\bar{r},\omega) B_n(\bar{r}) e^{i\omega\left(\frac{|\bar{r}-\bar{a}_n|}{c_l} - \delta_n\right)} + \bar{A}_n^{\perp}(\bar{r}) D_{Sn}(\bar{r},\omega) B_n(\bar{r}) e^{i\omega\left(\frac{|\bar{r}-\bar{a}_n|}{c_t} - \delta_n\right)} \Bigg\}. \tag{10}$$

sum of a linear incident field $\bar{u}^{(0)}$ and a secondary nonlinear component $\bar{u}^{(s)}$, such that

$$\bar{u}(t,\bar{r}) = \bar{u}^{(0)}(t,\bar{r}) + \bar{u}^{(s)}(t,\bar{r}). \tag{11}$$

The incident field is evaluated in the frequency domain from an analytical solution for a focused ultrasonic array. The model, which contains both longitudinal and shear field components, is expressed in Eq. (10).

Each element is considered to transmit with the same displacement amplitude Δ (defined as the peak amplitude one fundamental wavelength from the element center) and with a Gaussian spectra $T(\omega) = e^{-\alpha(\omega-\omega_0)^2}$ centered at the fundamental frequency w_0. The nth element has position a_n such that the amplitude unit vector of the longitudinal field component from each transmitting element is $\bar{A}_n(\bar{r}) = (\bar{r}-\bar{a}_n)/|\bar{r}-\bar{a}_n|$. Beam spread is accounted for by the term $B_n(\bar{r}) = |\bar{r}-\bar{a}_n|^{-\frac{1}{2}}$. The element directivity is approximated as the far-field response of a line source of width b acting on an elastic half-space [17]. These analytical solutions for the longitudinal and shear directivity functions are

$$D_{Ln}(\omega,\theta_n) = \operatorname{sinc}\left(\frac{\pi\omega b \sin\theta_n}{c_l}\right) \frac{\left((\frac{c_L}{c_S})^2 - 2\sin^2\theta_n\right)\cos\theta_n}{F_0(\sin\theta_n)}, \tag{12}$$

and

$$D_{Sn}(\omega,\theta_n) = \operatorname{sinc}\left(\frac{\pi\omega b \sin\theta_n}{c_t}\right) \frac{c_l}{c_s}^{5/2} \frac{\left((\frac{c_l}{c_s})^2 \sin^2\theta_n - 1\right)^{1/2} \sin 2\theta_n}{F_0(\frac{c_L}{c_S}\sin\theta_n)} \tag{13}$$

respectively, where

$$F_0(\zeta) = \left(2\zeta^2 - \left(\frac{c_L}{c_S}^2\right)\right)^2 - 4\zeta^2(\zeta^2-1)^{1/2}\left(\zeta^2 - \left(\frac{c_L}{c_S}\right)^2\right)^{1/2}. \tag{14}$$

Finally the element transmission delay is given by δ_n. For a focused longitudinal field in an isotropic material, $\delta_n = |\bar{a}_n - \bar{r}_f|/c_l$, where $\bar{r}_f$ is the focal position and c_l is the longitudinal velocity. The linear material parameters for aluminium are taken as; density ρ_o = 2700 kg/m^3, Young's modulus of E=90 GPa and Poisson's ratio ν = 0.35, which relate to the linear elastic moduli by $K = E/3(1-2\nu)$ and $\mu = E/2(1+\nu)$. The array parameters are selected to match the experiment and are $N = 64$, pitch w =0.63 mm, element width b=0.5 mm and center frequency ω_0=5 MHz. α is chosen such that the half power response corresponds to the manufacturer's stated frequency of $2/3\omega_0$. The third order elastic constants are taken as the following measured values for undamaged aluminium[18]; A= -344 GPa B= -124 GPa and C = -19.5 GPa.

B. Secondary field

Since the secondary field component is much smaller than the incident component, its contribution to the right hand side of Eq. (9) may be neglected. This allows the nonlinear forcing per unit volume to be approximated as Eq. (15). The secondary field component produced by this forcing may therefore be obtained from the solution of the following

$$\rho_0 \frac{\partial^2 u_i^{(s)}}{\partial t^2} - \mu \frac{\partial^2 u_i^{(s)}}{\partial x_k \partial x_k} - \left(K + \frac{\mu}{3}\right) \frac{\partial^2 u_l^{(s)}}{\partial x_l \partial x_i} = F_i. \tag{16}$$

This partial differential equation is solved numerically using a finite difference scheme. At each time step, t, the incident field described by Eq. (10) is evaluated as $\bar{u}^{(0)}(\bar{r},t) = \frac{1}{2\pi}\int_{-\infty}^{\infty} \bar{U}^{(0)}(\bar{r},\omega) e^{i\omega t}\, \mathrm{d}\omega$. The first and second order spatial derivatives of the incident field are then evaluated and from this the nonlinear forcing is computed. Numerical time-stepping is achieved using a fourth order Runge-Kutta method and all spatial derivatives are computed using fourth order finite difference approximations.

C. Imaging metric

Since a numerical integration step is required, the full nonlinear partial differential equation given by Eq. (9) could be solved directly in a similar manner without the requirement for perturbative approximations and producing a more accurate solution for the field. The motivation for this modeling is to evaluate the energy flux from the incident field both in terms of total magnitude and, importantly, where in space it occurs. By keeping the explicit separation of the incident and secondary field components this energy flux is more easily computed than if the field was modeled as a whole. In the approach taken here there is no nonlinear energy loss from the incident field. It may however be found implicitly by evaluating the nonlinear work done by the incident field on the secondary. This nonlinear work is equal to the energy flux that would occur from the incident to secondary field components and may be expressed as

$$
\begin{aligned}
F_i = &\left(\mu + \frac{A}{4}\right)\left(\frac{\partial^2 u_l^{(0)}}{\partial x_k \partial x_k}\frac{\partial u_l^{(0)}}{\partial x_i} + \frac{\partial^2 u_l^{(0)}}{\partial x_k \partial x_k}\frac{\partial u_i^{(0)}}{\partial x_l} + 2\frac{\partial^2 u_i^{(0)}}{\partial x_l \partial x_k}\frac{\partial u_l^{(0)}}{\partial x_k}\right) \\
&+ \left(K + \frac{\mu}{3} + \frac{A}{4} + B\right)\left(\frac{\partial^2 u_l^{(0)}}{\partial x_i \partial x_k}\frac{\partial u_l^{(0)}}{\partial x_k} + \frac{\partial^2 u_k^{(0)}}{\partial x_l \partial x_k}\frac{\partial u_i^{(0)}}{\partial x_l}\right) + \left(K - \frac{2}{3\mu} + B\right)\left(\frac{\partial^2 u_i^{(0)}}{\partial x_k \partial x_k}\frac{\partial u_i^{(0)}}{\partial x_l}\right). \\
&+ \left(\frac{A}{4} + B\right)\left(\frac{\partial^2 u_k^{(0)}}{\partial x_l \partial x_k}\frac{\partial u_l^{(0)}}{\partial x_i} + \frac{\partial^2 u_l^{(0)}}{\partial x_i \partial x_k}\frac{\partial u_k^{(0)}}{\partial x_k}\right) + (B + 2C)\left(\frac{\partial^2 u_k^{(0)}}{\partial x_i \partial x_k}\frac{\partial u_l^{(0)}}{\partial x_l}\right)
\end{aligned} \tag{15}
$$

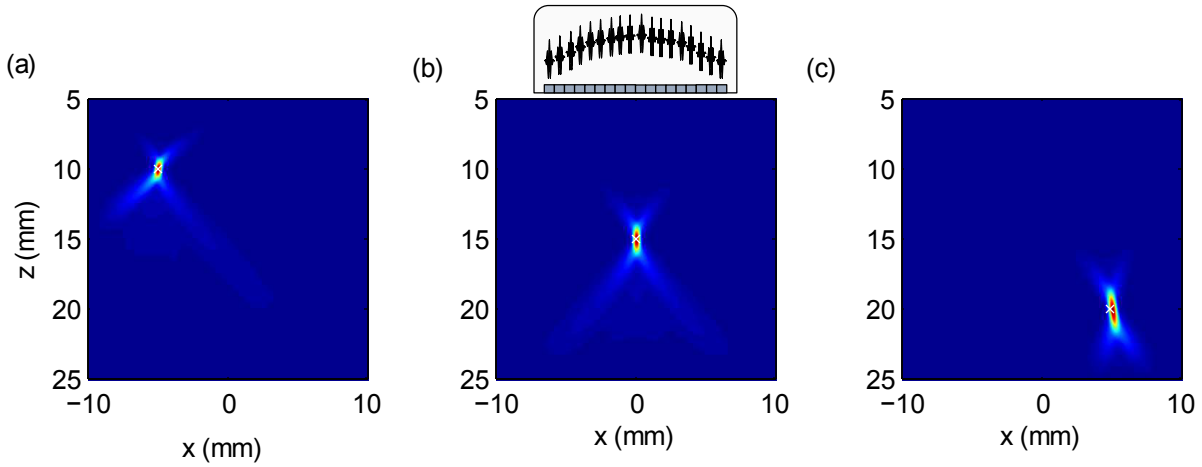

Fig. 4. Nonlinear weighting function $\Psi(\bar{r})$ for focal point of (a) $\bar{r}_f$=[-5 10] mm, (b) $\bar{r}_f$=[0 15] mm and (c) $\bar{r}_f$=[5 20] mm (focal points indicated by white cross).

$$
\Psi(\bar{r}) = \int_{t_1}^{t_2} \bar{F}(\bar{r}, t)\dot{\bar{u}}^{(s)}(\bar{r}, t)\ \mathrm{d}t, \tag{17}
$$

where t_1 and t_2 denote the time limits of the simulation, $\bar{F} = (F_i, F_j)$ is the nonlinear forcing vector and $\dot{\bar{u}}^{(s)}$ is the velocity vector of the secondary field component. The computed time window is chosen to be sufficiently long that the field propagates through the region of interest, which in this case corresponds to values to $t_1 = 0$ and $t_2 = 10\mu$s. Crucially evaluating the energy flux in this way allows it to be isolated for any point in space. This function provides insight into the degree of localization of the nonlinear measurement. Fig. 4 shows Eq. (17) evaluated for some example focal positions. This highlights that the imaging metric does not provide a point-like measurement of elastic nonlinearity but rather is a spatially averaged value that is weighted strongly to the focal point. This function is also closely related to the point spread function for the nonlinear imaging technique.

The total energy loss from the parallel transmission case may be obtained through the spatial integral of Eq. (17). This may then be related directly to the metric γ by evaluating the total energy flux in the parallel and sequential cases normalised to the total transmission energy, E_T. If $\Psi_s(\bar{r})$ denotes the spatial energy flux for the sequential transmission case, the contribution of elastic nonlinearity to the nonlinear imaging metric may be expressed as

$$
\eta(\bar{r}_f) = \frac{E_s - E_p}{E_s} = \frac{\int \Psi(\bar{r}_f, \bar{r})\ \mathrm{d}\bar{r} - \int \Psi_s(\bar{r})\ \mathrm{d}\bar{r}}{E_T}. \tag{18}
$$

Note that the sequential term in Eq. (18) is spatially invariant since all nonlinear losses occur during acquisition and are independent of the post-processed focusing operation. The total system energy is evaluated by applying Guass's theorem to the field described by Eq. (10). The energy transmitted by each element is obtained through a closed surface integral of acoustic intensity flux around the element. This may be written as follows

$$
E_T = N \int_{t_1}^{t_2} \oint (\bar{\sigma}^{(0)}\dot{\bar{u}}_l^{(0)}) \cdot \bar{n} + (\bar{\tau}^{(0)}\dot{\bar{u}}_s^{(0)}) \cdot \bar{n}^{\perp}\ \mathrm{d}s\ \mathrm{d}t, \tag{19}
$$

where $\bar{\sigma}^{(0)}$ and $\bar{\tau}^{(0)}$ are the field stresses due to the longitudinal and shear components respectively and $\bar{n}$ is the unit vector normal to the surface. The longitudinal and shear components of the particle velocities are denoted $\dot{\bar{u}}_l^{(0)}$ and $\dot{\bar{u}}_s^{(0)}$ respectively. Eq. (18) can be used to make predictions regarding the sensitivity of the imaging metric to elastic nonlinearity.

V. Nonlinear Sensitivity

A. Spatial sensitivity

By evaluating Eq. (18) for focal locations covering an imaging space, the dependence of the measured γ value on the location of the measurement point relative to the array

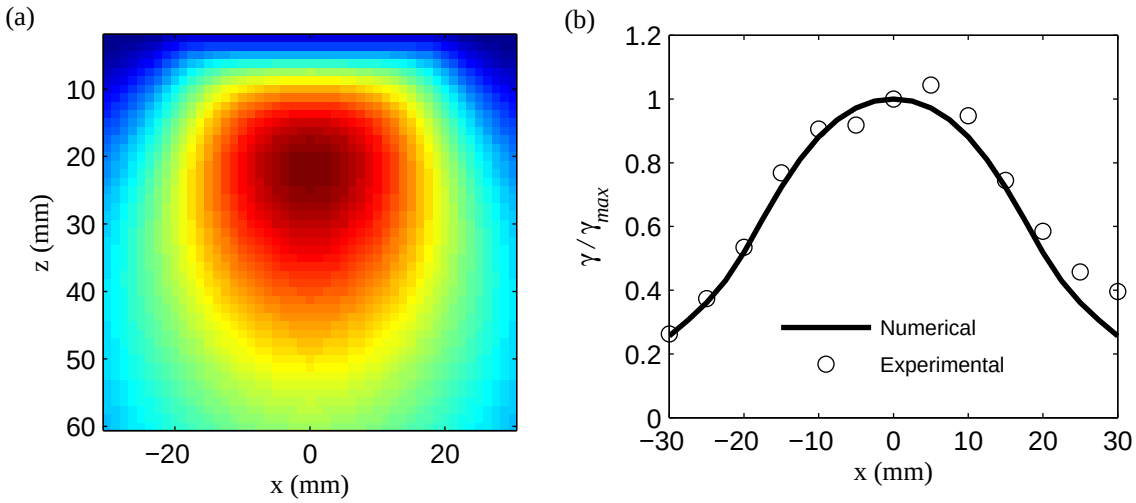

Fig. 5. Spatial variation of measured nonlinear response (a) numerical surface $\eta(\bar{r}_f)$ (b) Experimental and numerical lateral section for $z = 15$mm.

can be determined. This is shown in Fig. 5(a), from which it can be seen that the measured value for given elastic constants will vary as a function of position. This is primarily a consequence of variations in the intensity of the focused parallel field due to array directivity. Notably, as a result of higher order amplitude dependence, the region of insensitivity close to the array is more pronounced than is seen with linear imaging. This presents a potential practical challenge for near-surface nonlinear imaging. Fig. 5(a) also represents the expected image generated for uniform elastic nonlinearity if all other factors contributing to the measured γ value can be removed.

While it is difficult to experimentally validate the entire surface shown in Fig. 5(a), it is comparatively straight forward to acquire a lateral section of it. The fatigue crack specimen considered in the earlier example provides a discrete nonlinear elastic feature much stronger than the surrounding material. As such it can be used as a close experimental approximation to a point-like nonlinear feature. By acquiring a series of nonlinear images with the array translated relative to the crack position the lateral sensitivity can be examined. This translation is achieved by mechanically scanning the lateral position of the array along the surface of the specimen. Taking the peak nonlinear value from these images allows a section of the spatial variation surface to be populated at a depth equal to that of the crack tip. This is plotted in Fig. 5(b) alongside the numerical equivalent, both normalized to their peak values. Good agreement is seen between the two, providing a degree of validation for the numerical model.

This agreement also provides some insight into how the crack responds to a focused field. Since the model assumes an isotropic elastic nonlinearity, this result suggests there is no strong directivity associated with the nonlinear response of the crack. Despite the crack having a nominal direction of growth, its topography on the scale of the field displacements (which is the length scale at which nonlinear contact-acoustic effects occur and is in the order of nm) will be highly irregular. There would therefore be no strongly preferential direction for surface normals, resulting in the measurement being rather insensitive to the direction of the incident field. This is important since it reduces the effect of factors such as defect orientation on detectability. This is a proposed explanation for the observed agreement between the modeling and experimental results observed for the crack considered here. This study however does not provide sufficient evidence that this represents the general nonlinear response of fatigue cracks of any size and geometry.

B. N scaling

The dependence of the measured nonlinear response on the number of array elements and size of transmission aperture is now examined. Firstly the case of imaging within a scalar field is considered. For this example the total transmitted energy will be proportional to $N\Delta^2$. Neglecting effects of element directivity, the parallel focal amplitude is proportional to $N\Delta$. For some arbitrary quadratic nonlinearity β, the energy flux at the focal point for parallel transmission is proportional to $\beta N^4\Delta^4$ and for the sequential case is proportional to $\beta N\Delta^4$. For this simplified approximation the measured nonlinear value would be

$$\eta = \frac{E_s - E_p}{E_s} \propto \Delta^2(N^3 - 1)\beta. \tag{20}$$

It can be seen that for scalar field applications, such as biomedical imaging, the nonlinear diffuse energy measurement would have a cubic dependency on the number of transmitting elements. Consequently the sensitivity of the measurement could be expected to be improved to any arbitrary degree simply by increasing the number of array elements as illustrated in Fig 6(a).

The N scaling in application to nonlinear imaging of elastic solids is not so straight forward due to the manner in which

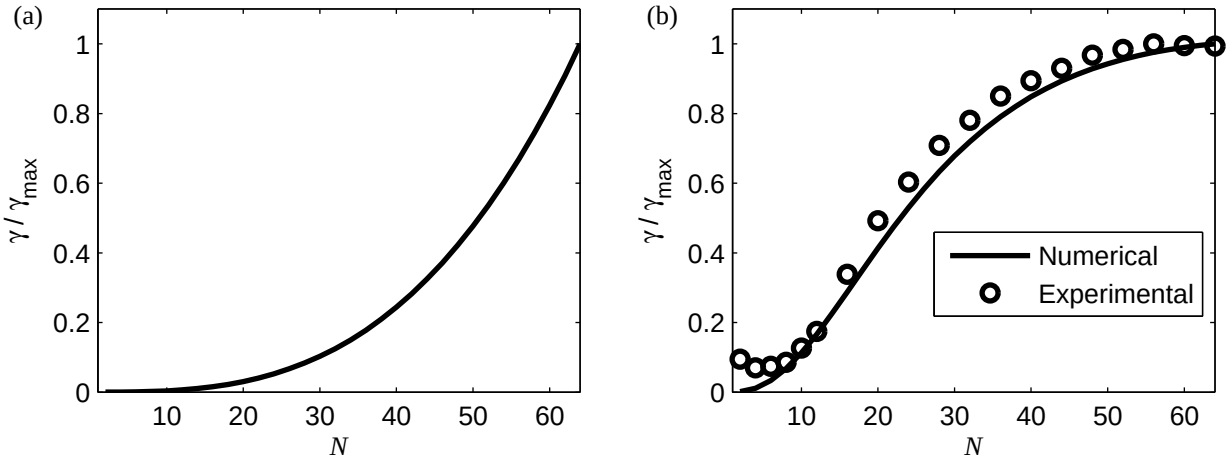

Fig. 6. Nonlinear amplitude γ variation with number of transmitting elements for (a) scalar field (b) vector field.

amplitude vectors interfere. Take the example of an array focused at a location below its center. At this focal position the vertical component of the amplitude vectors associated with the transmission of each element sum constructively, resulting in an increase in the stress seen by the material for parallel transmission. In this symmetric configuration the lateral components of the field interfere destructively thereby not contributing to any nonlinear energy flux in the parallel case. As the transmission aperture of the array is increased, the edge elements contribute an increasing proportion of their amplitude to the lateral direction. These additional elements therefore add little to absolute intensity at the focal point but do increase the total energy of the system. The consequence of this is a limit to sensitivity that can be achieved through increasing element number. Simulation results for the effect of element number are shown in Fig. 6(b). It is seen that initially the the nonlinear metric has a high order dependency on element number which then reduces as subsequent elements contribute increasingly less to the focal amplitude. Continuing to increase the aperture size further will in fact eventually reduce the measured nonlinear value as the total system energy increases linearly with element number, resulting in the existence of some optimal array size.

The effect of aperture size is also examined experimentally by monitoring the peak nonlinear response of the fatigue crack specimen as the number of elements used for transmission is increased symmetrically from the center of the array. This is shown normalized to the maximum value in Fig. 6(b) in which excellent agreement can be seen with the numerical results. As before, the good agreement with the model provides insight into the nonlinear response of the fatigue crack. The measured nonlinear response of the crack is dominated by non-classical contact acoustic effects as is evident by the significant subharmonic generation observed in similar specimens[19]. The modeling here assumes a classical form of nonlinearity which is not representative of the underlying nonlinear mechanics of a closed crack. The model therefore can not predict where, in terms of frequency or space, nonlinear energy flux occurs for such a defect. Despite this, the observed experimental agreement suggests that the nonlinear behavior in terms of total energy flux from the transmission bandwidth obeys quadratic amplitude scaling.

The smoothness of the function observed experimentally is perhaps unexpected since contact acoustic nonlinearity would be expected to exhibit some amplitude dependent thresholding behavior. One possible explanation for this observation could be, in a similar manner to the apparent isotropy of the response, that the smoothness is a consequence of the averaged effect of the complex geometry present at the scale of the displacements. Although any given contact point along the crack may exhibit its own thresholding behavior, because each contact point has a different orientation and local stress state, when the total effect is averaged over the order of a wavelength it behaves as a smooth function. The leveling off of the response around $N = 10$ is due to the limit of measurement sensitivity rather than an indication of thresholding behavior.

C. Amplitude dependence

The computed relationship between transmission amplitude Δ and the nonlinear metric is plotted in Fig. 7. As is consistent with the prediction of Eq. (20), γ is seen to be a quadratic function of transmission amplitude. These results are computed using third order elastic constants for undamaged aluminum and can therefore be used to predict the expected contribution of bulk material nonlinearity to the experimental baseline measurement. In order to relate these results to the experimental example considered here, the transmission amplitude must first be measured. A Polytec OFV-505 laser vibrometer was used to measure the back wall displacement of the test block in front of a single transmitting element. The model parameter Δ is defined as the displacement one fundamental wavelength in front of the element. After a correction is applied to the measured back wall displacement to account for beam spread the experimental Δ is found to be approximately 6nm.

As shown in Fig. 7(a), the predicted contribution from the bulk material nonlinearity of undamaged aluminium would be .07% ($\gamma = 0.0007$) for this excitation amplitude. As discussed

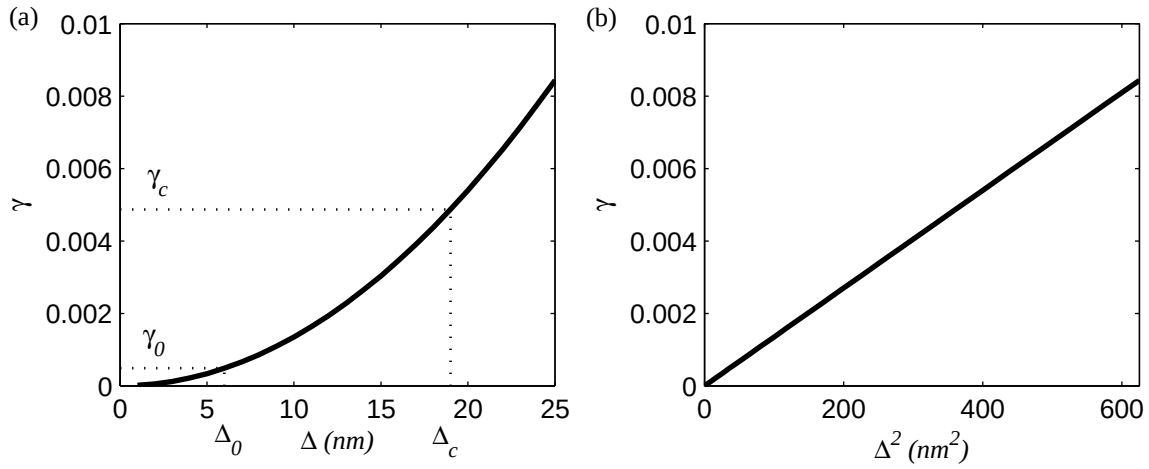

Fig. 7. Numerical γ dependence on excitation amplitude (a) Δ (b) Δ^2

in Sec. 3, the measured baseline value after the effect of noise has been removed is 0.5%, almost an order of magnitude larger than the predicted nonlinear material component. If all other factors have been accounted for then this disparity must be due to intrumentation error. Specifically this relates to the ability of the instrument to transmit identical energy in parallel and sequential transmission modes. This result would be indicative of a transmission energy close to 0.5% higher in the sequential transmission mode.

The nature of the diffuse measurement makes this technique uniquely suited to the the imaging of damage precursors since there is no requirement for the backscatter of sound from the inspection point. In order to detect damage precursors the experimental sensitivity to changes in third order elastic constants on the order of the undamaged material values is required [20], [21], [22]. The results presented here allow the required improvements in sensitivity to be quantified. As has been shown, sensitivity cannot be improved through increasing aperture or element numbers. One option for increasing sensitivity is to increases transmission amplitude. Fig. 7(a) shows that an amplitude increase of a little under three times the current value would provide the critical value, Δ_c, at which the bulk nonlinearity produces the largest single contribution to the measured baseline value. At this point changes in third order elastic constants would become measurable. Alternatively, measurement sensitivity may be improved through efforts to reduce or correct for instrument nonlinearity. If the nonlinear response of the instrumentation can be accurately characterized, most notably any differences in the energy transmitted in sequential and parallel operation modes, then corrections may be applied to the processing in order to remove these effects from the measurement.

VI. Conclusions

The factors contributing to the measured value obtained using the nonlinear ultrasonic diffuse energy imaging technique have been identified and characterized. Models have been presented for the effects of incoherent noise and elastic nonlinearity, the results of which are supported by experimental studies on the nonlinear imaging of fatigue cracks. The sensitivity, localization, spatial variability, aperture and amplitude dependence of the image metric are quantified. Insight has also been gained into the nonlinear response of fatigue cracks. It is seen that such defects exhibit a largely isotropic response for this imaging modality. Further, the total energy flux from the transmission bandwidth is seen to be well characterized using simple cubic approximations to strain energy. The ultimate aim of nonlinear imaging in application to nondestructive evaluation is to achieve the detection of damage precursors. This study identifies the experimental requirements necessary for that to be achieved. These results advance nonlinear diffuse energy imaging towards industrial viability.

Acknowledgments

The authors wish to acknowledge Jingwei Cheng for his assistance with some experimental measurements.

This work was supported by the UK Research Centre for Nondestructive Evaluation (RCNDE) and the Engineering and Physical Sciences Research Council (EPSRC) Grant EP/L022125/1.

References

[1] P. B. Nagy, "Fatigue damage assessment by nonlinear ultrasonic materials characterization," *Ultrasonics*, vol. 36, no. 1, pp. 375 – 381, 1998, ultrasonics International 1997. [Online]. Available: http://www.sciencedirect.com/science/article/pii/S0041624X97000401

[2] I. Solodov, N. Krohn, and G. Busse, "Can: an example of nonclassical acoustic nonlinearity in solids," *Ultrasonics*, vol. 40, no. 1, pp. 621 – 625, 2002. [Online]. Available: http://www.sciencedirect.com/science/article/pii/S0041624X02001865

[3] K. H. Matlack, J.-Y. Kim, L. J. Jacobs, and J. Qu, "Review of second harmonic generation measurement techniques for material state determination in metals," *Journal of Nondestructive Evaluation*, vol. 34, no. 1, p. 273, Nov 2014. [Online]. Available: https://doi.org/10.1007/s10921-014-0273-5

[4] G. L. Jones and D. R. Kobett, "Interaction of elastic waves in an isotropic solid," *The Journal of the Acoustical Society of America*, vol. 35, no. 1, pp. 5–10, 1963. [Online]. Available: http://dx.doi.org/10.1121/1.1918405

[5] A. J. Croxford, P. D. Wilcox, B. W. Drinkwater, and P. B. Nagy, "The use of non-collinear mixing for nonlinear ultrasonic detection of plasticity and fatigue," *The Journal of the Acoustical Society of America*, vol. 126, no. 5, pp. EL117–EL122, 2009. [Online]. Available: http://dx.doi.org/10.1121/1.3231451

[6] Y. Ohara, T. Mihara, R. Sasaki, T. Ogata, S. Yamamoto, Y. Kishimoto, and K. Yamanaka, "Imaging of closed cracks using nonlinear response of elastic waves at subharmonic frequency," *Applied Physics Letters*, vol. 90, no. 1, p. 011902, 2007. [Online]. Available: http://dx.doi.org/10.1063/1.2426891

[7] C.-S. Park, J.-W. Kim, S. Cho, and D. chul Seo, "A high resolution approach for nonlinear sub-harmonic imaging," *NDT & E International*, vol. 79, pp. 114 – 122, 2016. [Online]. Available: http://www.sciencedirect.com/science/article/pii/S0963869516000025

[8] P. Blanloeuil, L. Rose, J. Guinto, M. Veidt, and C. Wang, "Closed crack imaging using time reversal method based on fundamental and second harmonic scattering," *Wave Motion*, vol. 66, pp. 156 – 176, 2016. [Online]. Available: http://www.sciencedirect.com/science/article/pii/S0165212516300658

[9] Y. Ohara, K. Takahashi, Y. Ino, K. Yamanaka, T. Tsuji, and T. Mihara, "High-selectivity imaging of closed cracks in a coarse-grained stainless steel by nonlinear ultrasonic phased array," {*NDT*} *& E International*, vol. 91, pp. 139 – 147, 2017. [Online]. Available: http://www.sciencedirect.com/science/article/pii/S0963869517302359

[10] Y. Ohara, K. Takahashi, K. Jinno, and K. Yamanaka, "High-selectivity ultrasonic imaging of closed cracks using global preheating and local cooling," *MATERIALS TRANSACTIONS*, vol. 55, no. 7, pp. 1003–1010, 2014.

[11] S. Haupert, G. Renaud, and A. Schumm, "Ultrasonic imaging of nonlinear scatterers buried in a medium," *NDT & E International*, vol. 87, pp. 1 – 6, 2017. [Online]. Available: http://www.sciencedirect.com/science/article/pii/S0963869516303206

[12] J. N. Potter, A. J. Croxford, and P. D. Wilcox, "Nonlinear ultrasonic phased array imaging," *Phys. Rev. Lett.*, vol. 113, p. 144301, Oct 2014. [Online]. Available: https://link.aps.org/doi/10.1103/PhysRevLett.113.144301

[13] J. Cheng, J. N. Potter, A. J. Croxford, and B. W. Drinkwater, "Monitoring fatigue crack growth using nonlinear ultrasonic phased array imaging," *Smart Materials and Structures*, vol. 26, no. 5, p. 055006, 2017. [Online]. Available: http://stacks.iop.org/0964-1726/26/i=5/a=055006

[14] C. Holmes, B. W. Drinkwater, and P. D. Wilcox, "Post-processing of the full matrix of ultrasonic transmitreceive array data for non-destructive evaluation," *NDT & E International*, vol. 38, no. 8, pp. 701 – 711, 2005. [Online]. Available: http://www.sciencedirect.com/science/article/pii/S0963869505000721

[15] L. Landau and E. Lifshitz, in *Theory of Elasticity (Third Edition)*. Butterworth-Heinemann, 1986. [Online]. Available: http://www.sciencedirect.com/science/article/pii/B9780080570693500048

[16] F. D. Murnaghan, "Finite deformations of an elastic solid," *American Journal of Mathematics*, vol. 59, no. 2, pp. 235–260, 1937. [Online]. Available: http://www.jstor.org/stable/2371405

[17] G. F. Miller and H. Pursey, "The field and radiation impedance of mechanical radiators on the free surface of a semi-infinite isotropic solid," *Proceedings of the Royal Society of London A: Mathematical, Physical and Engineering Sciences*, vol. 223, no. 1155, pp. 521–541, 1954. [Online]. Available: http://rspa.royalsocietypublishing.org/content/223/1155/521

[18] V. Lubarda, "New estimates of the third-order elastic constants for isotropic aggregates of cubic crystals," *Journal of the Mechanics and Physics of Solids*, vol. 45, no. 4, pp. 471 – 490, 1997. [Online]. Available: http://www.sciencedirect.com/science/article/pii/S0022509696001135

[19] J. N. Potter, J. Chen, A. J. Croxford, and B. W. Drinkwater, "Ultrasonic phased array imaging of contact-acoustic nonlinearity," *Proceedings of Meetings on Acoustics*, vol. 29, no. 1, p. 045002, 2016. [Online]. Available: http://asa.scitation.org/doi/abs/10.1121/2.0000409

[20] J.-Y. Kim, L. J. Jacobs, J. Qu, and J. W. Littles, "Experimental characterization of fatigue damage in a nickel-base superalloy using nonlinear ultrasonic waves," *The Journal of the Acoustical Society of America*, vol. 120, no. 3, pp. 1266–1273, 2006. [Online]. Available: http://dx.doi.org/10.1121/1.2221557

[21] J.-Y. Kim, J. Qu, L. J. Jacobs, J. W. Littles, and M. F. Savage, "Acoustic nonlinearity parameter due to microplasticity," *Journal of Nondestructive Evaluation*, vol. 25, no. 1, pp. 28–36, Mar 2006. [Online]. Available: https://doi.org/10.1007/s10921-006-0004-7

[22] K. H. Matlack, J. J. Wall, J.-Y. Kim, J. Qu, L. J. Jacobs, and H.-W. Viehrig, "Evaluation of radiation damage using nonlinear ultrasound," *Journal of Applied Physics*, vol. 111, no. 5, p. 054911, 2012. [Online]. Available: http://dx.doi.org/10.1063/1.3692086